Published in IET Electric Power Applications
Received on 25th June 2007
Revised on 4th January 2008
doi: 10.1049/iet-epa:20070281


ISSN 1751-8660

# Analysis of a short-stroke, single-phase, quasi-Halbach magnetised tubular permanent magnet motor for linear compressor applications

*J. Wang Z. Lin D. Howe*

*Department of Electronic and Electrical Engineering, University of Sheffield, Mappin Street, Sheffield S1 3JD, UK*
*E-mail: j.b.wang@sheffield.ac.uk*

**Abstract:** The analysis of a novel single-phase, short-stroke, reciprocating tubular motor with a quasi-Halbach magnetised moving-magnet armature is described. The motor was developed for applications such as linear compressors. The magnetic field distribution, the back-emf and the thrust force of the motor are established analytically in the cylindrical co-ordinate system, and predictions are compared with results derived from finite-element (FE) analysis. It is shown that the difference between the analytical and FE predicted average emf (thrust force) over the operating stroke of 0.01 m is $<5\%$. The analysis and the emf and thrust force predictions are validated by measurements.

## 1 Introduction

Conventional refrigerator compressors comprise a rotary electric motor (usually induction motor) that drives a reciprocating pump through a crank. Their overall efficiency is, however, relatively low, due to the inherently low efficiency of induction motors and the mechanical friction that is associated with the crank-driven piston. A reciprocating compressor driven by a linear motor [1, 2] eliminates the side force on the cylinder wall caused by the crank shaft, and therefore not only significantly reduces the frictional loss, but also makes it possible to operate without a lubricant. A unique feature of such a linear compressor is the fact that the piston amplitude can be readily varied, whereas in a conventional compressor, in which the crank converts rotary-to-linear motion, the stroke is fixed. This provides a simple means for modulating the refrigerator load according to the demand and results in additional energy saving.

Various linear machine technologies and topologies might be employed in reciprocating linear compressor applications. The main technologies are induction machines, permanent magnet (PM) machines and switched reluctance machines [3]. However, due to their significantly higher efficiency, PM excited machines are deemed to be most appropriate for the proposed compressor applications. Of the possible topologies, tubular configurations are compatible with the packaging/integration requirements of vapour compressors – since they have zero net radial force between the armature and the stator, no end-windings, and are volumetrically efficient [4–7]. These may be classified as moving-coil, moving-iron and moving-magnet. However, only moving-magnet topologies [8–11] have the necessary high force capability per moving mass, which is essential to facilitate resonant operation at the electrical supply frequency with minimum spring stiffness.

A single-phase, moving-magnet tubular motor topology [1] which is commonly adopted for reciprocating applications is shown in Fig. 1, the stator core and the stationary back iron being laminated in the circumferential direction. It is a homopolar motor in which the magnet is radially magnetised. Consequently, the majority of the magnet flux returns via the surrounding air. This not only results in a very poor force capability but also an additional

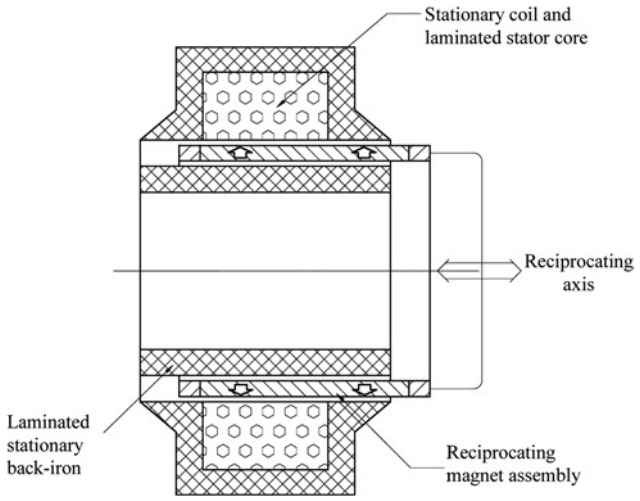


**Figure 1** *Single-phase, tubular moving-magnet motor with homopolar radially magnetised magnets and stationary back-iron*

eddy current loss in the magnet and surrounding metallic structure, induced by the reciprocating movement of the magnet. Hence, the overall motor efficiency is greatly compromised. Further, while the moving mass of the motor is reduced by employing stationary armature back-iron, as shown in Fig. 1, this introduces an additional air-gap and makes the realisation of an integrated linear motor/compressor unit significantly more complicated, which has cost implications.

This paper proposes a new tubular, PM motor topology, as shown in Fig. 2, for linear compressor applications. It employs a 2-pole quasi-Halbach magnetised armature, having radially magnetised ring magnets placed at the centre and both ends, and a soft magnetic composite (SMC) stator core which carries a single-phase coil. Such a coil is easy to manufacture and results in a very high packing factor, which is conducive to high efficiency. The quasi-Halbach magnetised armature generates a magnetic field which is linked with the single-phase stator coil. Reciprocating thrust force is produced as the result of the interaction between the permanent magnetic field and the stator current when it is synchronised with the armature movement. Unlike the homopolar motor shown in Fig. 1, the flux due to PMs returns through the back-iron of the armature, and therefore the stationary back iron is not needed and the second air-gap is eliminated. This not only improves the thrust force capability of the motor, but also greatly reduces the eddy current loss due to stray magnetic field in the surrounding metallic structure. A unique feature of the quasi-Halbach magnetisation is that the axially magnetised magnets essentially provide a return path for the radial air-gap flux, and hence, the flux in the inner bore of the magnets is relatively small. As a result, the use of a very thin ferromagnetic tube or even a non-magnetic tube on which to mount the magnets will not significantly compromise the thrust force capability. Thus, the specific force capability and, hence, the efficiency of the proposed motor are significantly better than that of the motor shown in Fig. 1.

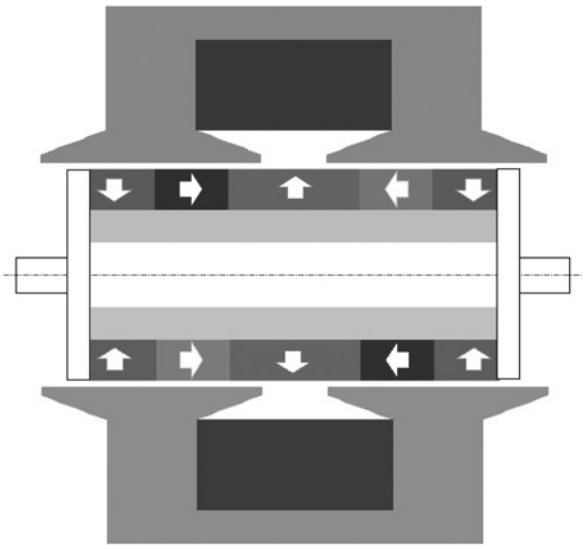

**Figure 2** *Schematic of single-phase, quasi-Halbach magnetised, tubular motor*

## 2 Open-circuit magnetic field distribution

In order to establish an analytical expression for the magnetic field distribution in the tubular motor shown in Fig. 2, the following assumptions are made:

(i) The stator is slotless and the permeability of the iron is infinite. However, slotting effects can be taken into account by introducing a Carter coefficient, as has been shown in [12].

(ii) The axial length of the tubular motor is infinite and comprises an infinitely long iron sleeve and a series of PM armatures, which are separated by the axial distance $\tau_l$ and which extend to infinity along the machine axis, as illustrated in Fig. 3.

Assumption (ii) is justified by the fact that the stator is axially longer than the moving-magnet armature such that at the rated stroke range the magnet armature extends only slightly beyond the stator iron, as can be seen in Fig. 9*b*. The magnetic field model of the actual tubular motor may be represented by one of the repetitive elements shown in Fig. 3, provided that the separation distance $\tau_l$ between two adjacent armatures is much greater than the pole-pitch $\tau_p$, that is, $\tau_l \gg \tau_p$ [13]. Consequently, the magnetic field analysis is confined to the airspace regions I and III in which the permeability is $\mu_0$ and the PM region II in which the permeability is $\mu_0\mu_r$, where $\mu_r$ is the relative recoil permeability. However, to simplify the analysis, regions II and III are combined by assuming that



doi: 10.1049/iet-epa:20070281

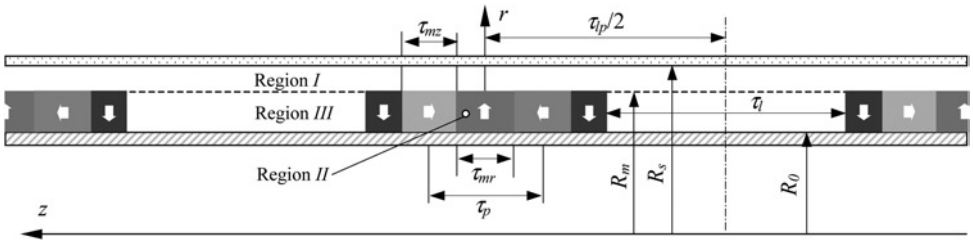


**Figure 3** *Analytical field model*

$\mu_{II} = \mu_{III} = \mu_0$. This is justified since NdFeB magnets are to be employed, for which $\mu_r = 1.05$. Thus, effectively, the airspace between the PM armatures is assumed to be occupied by PM material, but the magnets are only magnetised in region II, and are un-magnetised in region III. The governing field equations, in terms of the vector magnetic potential $A_\theta$, are

$$\begin{cases} \dfrac{\partial}{\partial z}\left(\dfrac{1}{r}\dfrac{\partial}{\partial z}(rA_{I\theta})\right) + \dfrac{\partial}{\partial r}\left(\dfrac{1}{r}\dfrac{\partial}{\partial r}(rA_{I\theta})\right) = 0 \\ \dfrac{\partial}{\partial z}\left(\dfrac{1}{r}\dfrac{\partial}{\partial z}(rA_{II,III\theta})\right) + \dfrac{\partial}{\partial r}\left(\dfrac{1}{r}\dfrac{\partial}{\partial r}(rA_{II,III\theta})\right) = -\mu_0 \nabla \times \boldsymbol{M} \end{cases} \tag{1}$$

In the cylindrical co-ordinate system, the magnetisation $\boldsymbol{M}$ is given by

$$\boldsymbol{M} = M_r \mathbf{e}_r + M_z \mathbf{e}_z \tag{2}$$

where $M_r$ and $M_z$ denote the components of $\boldsymbol{M}$ in the $r$ and $z$ coordinate directions, respectively. Fig. 4 shows the distribution of $M_r$ and $M_z$, where $\tau_{mr}$ and $\tau_{mz}$ are the axial lengths of the radially and axially magnetised magnets on the quasi-Halbach magnetised armature, respectively, their sum being equal to the pole-pitch, that is, $\tau_p = \tau_{mr} + \tau_{mz}$, whereas $\tau_{lp} = 2\tau_p + \tau_l$ is the fundamental period of the magnetisation. The magnetisation distribution may be expanded into a Fourier series. Thus, $M_r$ and $M_z$ may be expressed as functions of $z$

$$M_r = \sum_{n=1,2,\ldots}^{\infty} M_{rn} \cos\, m_n z \;;\; M_z = \sum_{n=1,2,\ldots}^{\infty} M_{zn} \sin\, m_n z \tag{3}$$

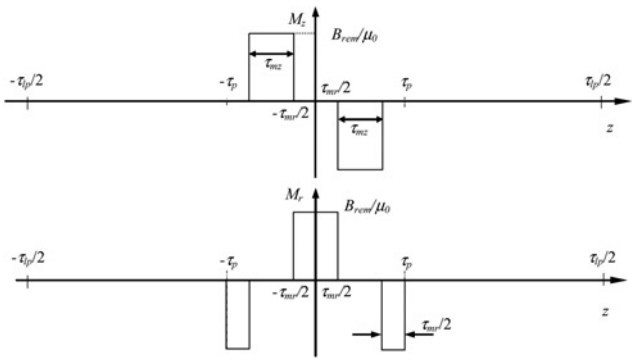


**Figure 4** *Magnetisation distributions*

where

$$\begin{aligned} m_n &= 2\pi n/\tau_{lp} \\ M_{rn} &= -\frac{2B_{rem}}{\mu_0 \pi n}\left[\sin\frac{m_n\tau_{mr}}{2} - \sin\, m_n\tau_p + \sin\, m_n\left(\tau_{mz} + \frac{\tau_{mr}}{2}\right)\right] \\ M_{zn} &= -\frac{4B_{rem}}{\mu_0 \pi n}\sin\frac{m_n\tau_{mz}}{2}\sin\frac{m_n\tau_p}{2} \end{aligned} \tag{4}$$

and $B_{rem}$ is the magnet remanenc. Thus, (1) may be re-written as

$$\begin{cases} \dfrac{\partial}{\partial z}\left(\dfrac{1}{r}\dfrac{\partial}{\partial z}(rA_{I\theta})\right) + \dfrac{\partial}{\partial r}\left(\dfrac{1}{r}\dfrac{\partial}{\partial r}(rA_{I\theta})\right) = 0 \\ \dfrac{\partial}{\partial z}\left(\dfrac{1}{r}\dfrac{\partial}{\partial z}(rA_{II\theta})\right) + \dfrac{\partial}{\partial r}\left(\dfrac{1}{r}\dfrac{\partial}{\partial r}(rA_{II\theta})\right) = \displaystyle\sum_{n=1}^{\infty} P_n \sin\, m_n z \end{cases} \tag{5}$$

where

$$P_n = \frac{4B_{rem}}{\tau_{lp}}\left[\sin\, m_n\frac{\tau_{mr}}{2} - \sin\, m_n\tau_p + \sin\, m_n\left(\tau_{mz} + \frac{\tau_{mr}}{2}\right)\right] \tag{6}$$

It should be noted that the foregoing treatment of the magnetisation makes it possible to derive an analytical solution for the magnetic field distribution of the short-stroke PM motor using the techniques described in [12] subject to the following boundary conditions

$$\begin{aligned} B_{zI}\big|_{r=R_S} &= 0 \quad ; \quad H_{zII}\big|_{r=R_0} = 0 \\ B_{rI}\big|_{r=R_m} &= B_{rII}\big|_{r=R_m} \quad ; \quad H_{zI}\big|_{r=R_m} = H_{zII}\big|_{r=R_m} \end{aligned} \tag{7}$$

The resulting expressions for the flux density components are given by

$$\begin{aligned} B_{Ir}(r,z) &= -\sum_{n=1,2,\ldots}^{\infty}\left[a_{In}BI_1(m_n r) + b_{In}BK_1(m_n r)\right]\cos(m_n z) \\ B_{Iz}(r,z) &= \sum_{n=1,2,\ldots}^{\infty}\left[a_{In}BI_0(m_n r) - b_{In}BK_0(m_n r)\right]\sin(m_n z) \end{aligned} \tag{8}$$

$$B_{\mathrm{II}r}(r,z) = -\sum_{n=1,2,\ldots}^{\infty} \{[F_{An}(m_n r) + a_{\mathrm{II}n}]BI_1(m_n r) + [-F_{Bn}(m_n r) + b_{\mathrm{II}n}]BK_1(m_n r)\}\cos(m_n z)$$
$$B_{\mathrm{II}z}(r,z) = \sum_{n=1,2,\ldots}^{\infty} \{[F_{An}(m_n r) + a_{\mathrm{II}n}]BI_0(m_n r) - [-F_{Bn}(m_n r) + b_{\mathrm{II}n}]BK_0(m_n r)\}\sin(m_n z) \quad (9)$$

where $BI_0(\bullet)$, $BI_1(\bullet)$ are modified Bessel functions of the first kind; $BK_0(\bullet)$, $BK_1(\bullet)$ are modified Bessel functions of the second kind, of order 0 and 1, respectively; and $F_{An}(\bullet)$, $F_{Bn}(\bullet)$, $a_{\mathrm{I}n}$, $b_{\mathrm{I}n}$, $a_{\mathrm{II}n}$ and $b_{\mathrm{II}n}$ are given in Appendix A in [14]. However, $P_n$ and $B_n$ should be calculated using (6) and the expression given below, respectively.

$$B_n = \frac{-4B_{\mathrm{rem}}}{\mu_r n\pi}\sin\frac{m_n\tau_{\mathrm{p}}}{2}\sin\frac{m_n\tau_{mz}}{2}$$

## 3 Flux-linkage, emf and thrust force

The flux-linkage with the stator coil may be obtained by the following integration

$$\Psi_{\mathrm{c}} = \frac{N_{\mathrm{c}}}{b_0}\int_{\tau_{\mathrm{wp}}-b_0/2-z_{\mathrm{d}}}^{\tau_{\mathrm{wp}}+b_0/2-z_{\mathrm{d}}} 2\pi R_s A_{\mathrm{I}\theta}(R_s, z)\,\mathrm{d}z \quad (10)$$

where $N_{\mathrm{c}}$ is the number of turns, $b_0$ is the width of the stator slot opening, $\tau_{wp}$ is the axial position of the coil centre and $z_{\mathrm{d}}$ is the axial displacement of the PM armature, as shown in Fig. 5.

Application of (10) yields

$$\Psi_{\mathrm{c}} = \sum_{n=1}^{\infty}\Phi_{wn}\sin m_n z_{\mathrm{d}} \quad (11)$$

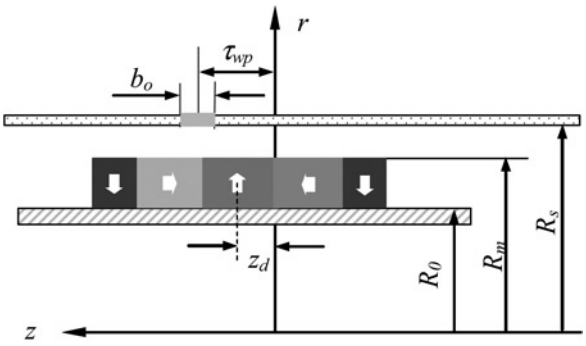


**Figure 5** *Relative position of coil and armature*

where

$$\Phi_{wn} = 2\pi N_{\mathrm{c}} K_{rn} K_{\mathrm{dp}n}/m_n$$

$$K_{rn} = R_s[a_{\mathrm{I}n}BI_1(m_n R_s) + b_{\mathrm{I}n}BK_1(m_n R_s)] \quad (12)$$

$$K_{\mathrm{dp}n} = \frac{\sin m_n b_0/2}{m_n b_0/2} \quad (13)$$

The induced emf is obtained as

$$e_w = -\frac{\mathrm{d}\Psi_{\mathrm{c}}}{\mathrm{d}t} = -\left(\sum_{n=1}^{\infty} K_{\mathrm{E}n}\cos m_n z_{\mathrm{d}}\right)\frac{\mathrm{d}z_{\mathrm{d}}}{\mathrm{d}t} = K_{\mathrm{E}}(z_{\mathrm{d}})v \quad (14)$$

where $K_{\mathrm{E}}(z_{\mathrm{d}})$, defined as the back-emf coefficient of the motor, is dependent on the displacement of the PM armature and $v$ is the velocity of the armature. $K_{\mathrm{E}n}$ is given by

$$K_{\mathrm{E}n} = 2\pi N_{\mathrm{C}} K_{rn} K_{\mathrm{dp}n} \quad (15)$$

The instantaneous thrust force, $F_{\mathrm{T}}$, when the stator winding carries a current $i$ is obtained from

$$F_{\mathrm{T}} = ei/v = K_{\mathrm{E}}(z_{\mathrm{d}})i = K_{\mathrm{T}}(z_{\mathrm{d}})i \quad (16)$$

where $K_{\mathrm{T}}(z_{\mathrm{d}})$, defined as the thrust force coefficient of the motor, is identical to $K_{\mathrm{E}}(z_{\mathrm{d}})$ and is also dependent on the displacement of the PM armature.

The flux that passes through the back-iron of the PM armature is given by

$$\Phi_{\mathrm{b}} = 2\pi R_0 A_{\theta\mathrm{II}}(R_0, z) = 2\pi R_0\sum_{n=1,2,\ldots}^{\infty}\frac{1}{m_n}\{a_{\mathrm{II}n}BI_1(m_n r) + b_{\mathrm{II}n}BK_1(m_n r)\}\sin(m_n z) \quad (17)$$

This equation can be used to determine the required radial thickness of the ferromagnetic support tube.

## 4 Comparison with FE analysis

The design parameters of a single-phase, short-stroke, tubular PM machine having the topology shown in Fig. 2 and a performance which meets the requirements of a typical domestic refrigerator compressor, are given in Table 1. The sintered NdFeB magnets, for which $B_{\mathrm{rem}} = 1.04$ T and $\mu_{\mathrm{r}} = 1.05$, are mounted on a mild steel tube, whereas the SMC stator core is manufactured from Somaloy 700$^{\mathrm{TM}}$ [15]. The analytically derived flux density

**Table 1** Design parameters of single-phase, short-stroke, tubular PM motor, m

| $R_e$ | $R_s$ | $R_m$ | $R_0$ | $h_t$ |
|---|---|---|---|---|
| 0.04 | 0.0208 | 0.02 | 0.015 | 0.001 |
| $B_0$ | $\tau_{\mathrm{p}}$ | $\tau_{mr}$ | $\tau_{mz}$ | $\alpha$ |
| 0.008 | 0.025 | 0.016 | 0.009 | 20° |




doi: 10.1049/iet-epa:20070281

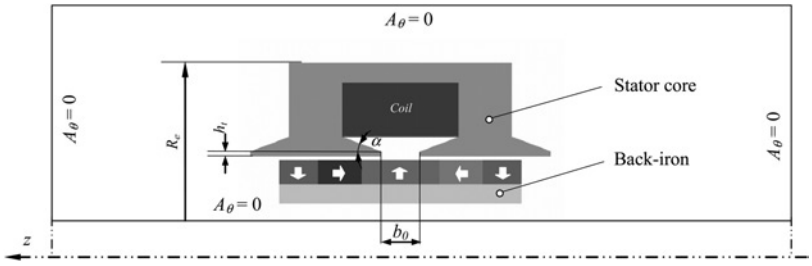


**Figure 6** *FE model*

components have been compared with those deduced from axisymmetric finite-element (FE) analysis.

Non-linear FE analysis was carried out using the model shown in Fig. 6, in which the Dirichlet condition is imposed on the enclosing boundary and appropriate $B-H$ curves were assumed for the SMC and mild steel ferromagnetic materials. The model accounts for all the key features of the motor, such as, the finite axial lengths of the stator and armature, as well as saturation. Fig. 7 shows the $B-H$ curves of the magnets, Somaloy$^{TM}$ 700 SMC and mild-steel used in the FE analysis, all of which are treated as being isotropic.

Fig. 8 compares the analytically predicted and FE calculated distributions of the no-load radial and axial flux density components, $B_{Ir}$ and $B_{Iz}$, in the air-gap as a function of the axial position z, at radius = 0.02043 m for

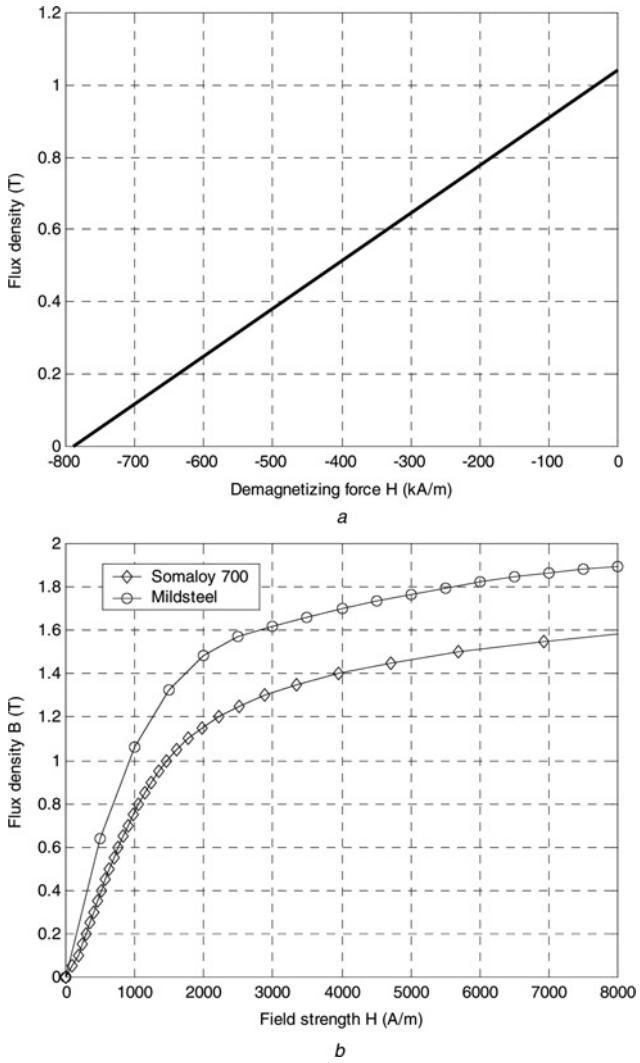


**Figure 7** *B–H curves used in FE analysis*

*a* NdFeB at 100 °C
*b* Somaloy 700 and mildsteel

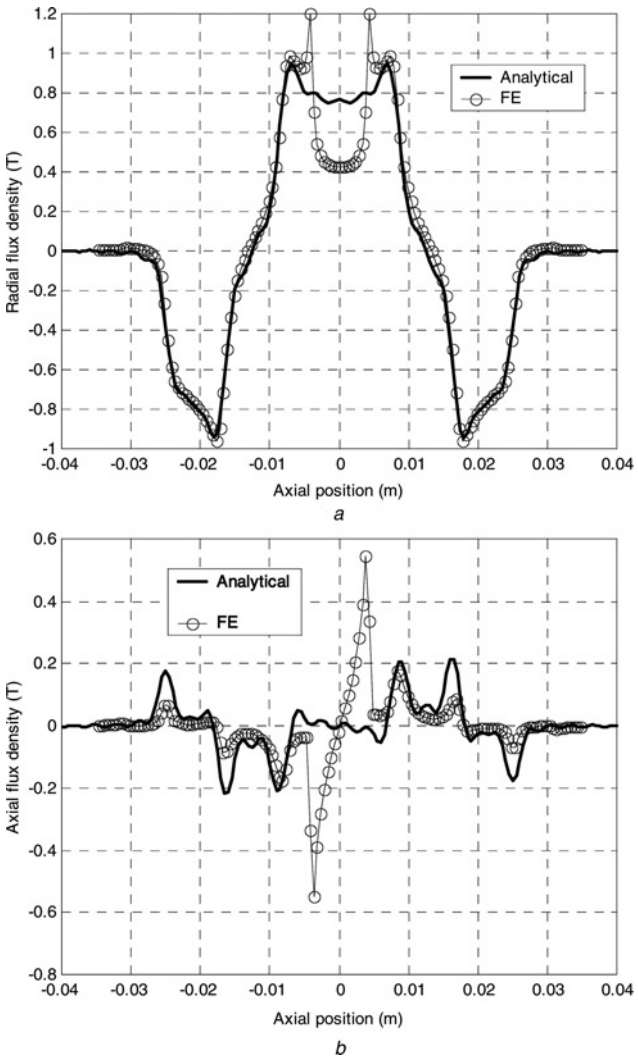


**Figure 8** *Comparison of no-load flux density components in air-gap (at $r = 0.02043$ and $z_d = 0$) as a function of z*

*a* Radial component
*b* Axial component

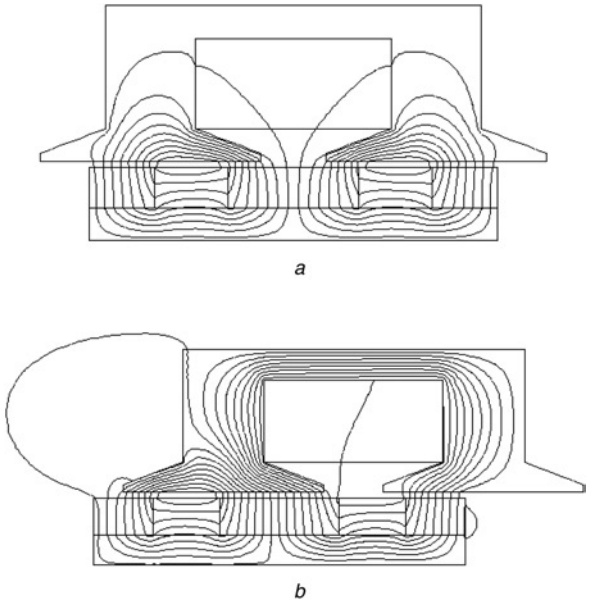


**Figure 9** *Flux distributions*
*a* At $z_d = 0$
*b* At $z_d = 0.01$ m

zero axial displacement ($z_d = 0$) between the stator and the PM armature. Fig. 9 shows FE calculated flux distributions for zero displacement and maximum displacement ($Z_d = 0.01$ m) of the armature, whereas Fig. 10 compares the analytically predicted and FE calculated induced emf as a function of the armature displacement, at an armature velocity of 3 m/s. As will be seen, the analytical solutions agree well with the FE predictions, the main discrepancy being in regions close to the slot opening, which is not taken into account in the analytical model other than by the use of a Carter coefficient.

Due to the relatively wide stator slot opening, the FE predicted reduction in the radial flux density in the vicinity of the slot opening is more pronounced than that which is predicted analytically. Consequently, the FE predicted emf is lower than the analytical prediction when the armature displacement is less than 0.0045 m. As the armature displacement increases, however, this trend is reversed due to the effect of fringing flux associated with the finite length stator core [16]. The difference in the analytical and FE predicted average emfs over a stroke range of 0.01 m is, however, <5%.

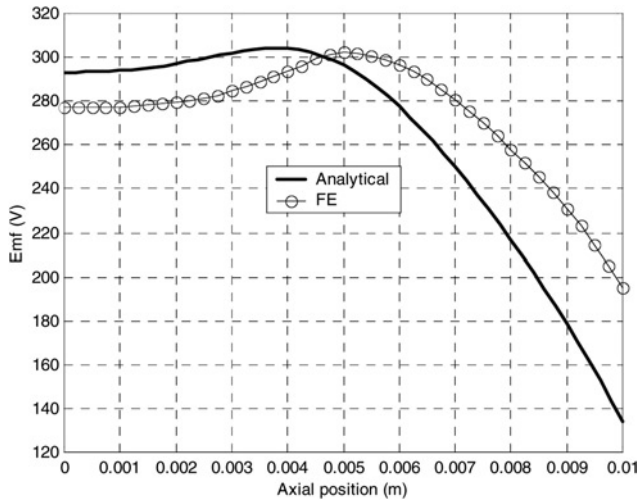


**Figure 10** *Comparison of emfs as a function of armature displacement at $v = 3$ m/s*

It should be noted that in order to reduce the eddy current loss in the moving magnet armature, both magnets and the back-iron are axially and circumferentially segmented. Consequently, the effect of eddy current in the magnets and back-iron of the motor on thrust force is negligible [17].

## 5 Experimental results

Fig. 11 shows a prototype of the motor whose design parameters are given in Table 1 mounted on a test rig. It also shows the excitation coil, the two identical SMC parts which from the stator core, and the moving-magnet armature with quasi-Halbach magnetised sintered NdFeB magnets.

The variation of the open-circuit flux-linkage of the prototype motor as a function of the armature displacement was measured by a flux-meter, whereas the armature displacement was adjusted by a micrometer barrel, shown on the left of the test rig, and the armature position was measured by an a Linear Variable Differential Transformer, mounted on the right of the rig. The thrust force was measured by a force transducer mounted between the micrometer barrel and the motor shaft. In order to obtain the net thrust force, the variation of the cogging force with armature position was first measured with the motor on open-circuit. The measurements were then repeated for different values of excitation current. The net thrust for a given current and armature displacement was then obtained by subtracting the measured cogging force from the total force. Fig. 12 compares the measured and FE predicted flux-linkage – armature displacement characteristics, whereas Fig. 13 compares the variation of the FE and analytically predicted and measured thrust force for an excitation current of 1.0 A. As will be seen, the measurements agree well with the FE predictions. The

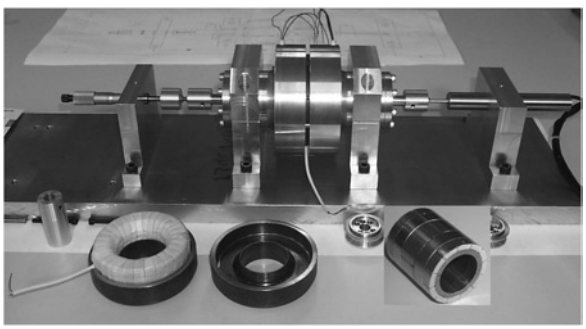

**Figure 11** *Prototype tubular motor and test rig*




doi: 10.1049/iet-epa:20070281

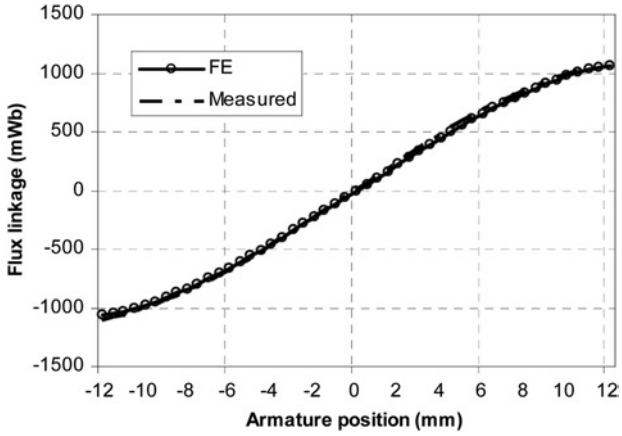


**Figure 12** *Variation of measured and predicted flux-linkage with armature displacement*

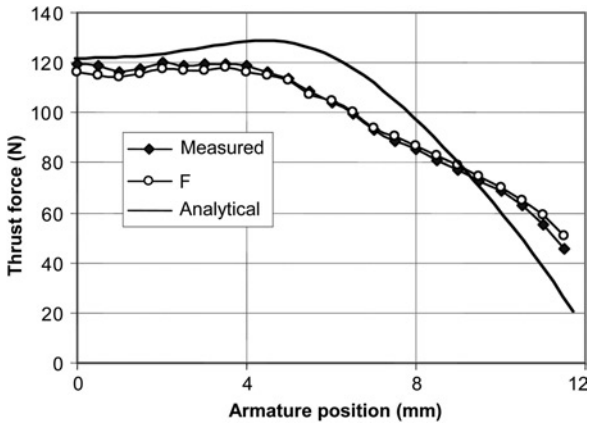


**Figure 13** *Variation of measured and predicted thrust force with armature displacement for an excitation current of 1.0 A*

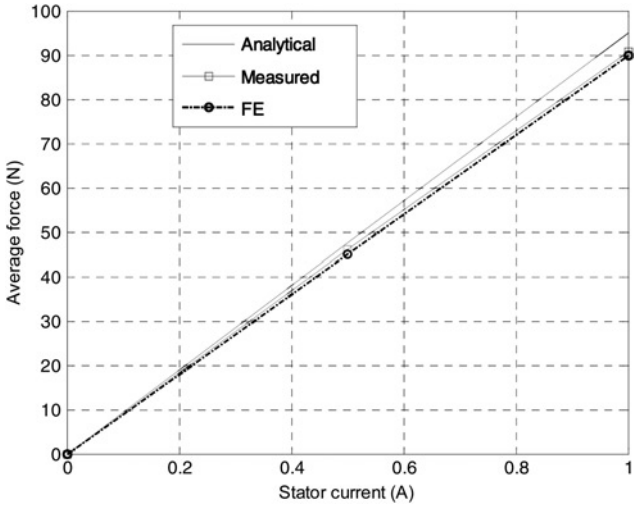


**Figure 14** *Variation of measured and predicted average thrust force over stroke range with stator current*

difference in the analytically predicted and measured average thrust force over the stroke range is 5.5%, being slightly greater than that in the back-emfs of Fig. 10. Fig. 14 compares the measured and predicted average thrust force over the stroke range as functions of motor current. As can be seen, the average thrust force is virtually linearly proportional to excitation current up to the maximum peak value of 1.0 A at which the machine is designed to operate.

A comparative study has also been undertaken to establish the force capability of the conventional design, shown in Fig. 1, with the same volumetric and thermal constraints as the prototype motor. The homopolar motor employs the same grade and thickness of magnets and has two 0.8 mm air-gaps. The other dimensions are optimised, which yields an average force over the stroke being 15.5% less than that of the prototype motor. This will translate into 1.5–2% reduction in efficiency.

## 6 Conclusion

A short-stroke, single-phase, quasi-Halbach magnetised tubular PM motor has been proposed for linear refrigerator compressor applications. Analytical formulae for predicting the open-circuit magnetic field distribution, the back-emf and the thrust force have been established. The utility and accuracy of the analytically derived formulae have been demonstrated by comparing with results deduced from FE analysis. It has been shown that the difference between the analytical and FE predicted average emfs over the rated stroke of 0.01 m is $<5\%$. The analysis and the emf and thrust force predictions have also been validated by measurements. The developed analytical tool should provide a useful aid for the design optimisation of linear compressor systems.

## 7 Acknowledgment

The work that is described in this paper was undertaken in a project which was part-funded by the Carbon Trust. The authors would like to thank other project partners, Indesit UK Ltd, Magnet Applications Ltd, UK, Hoganas AB, Sweden and Danfoss Compressors GmbH, Germany for permission to publish the paper.

## 8 References

[1] PARK K., HONG E.P., LEE K.H.: 'Development of a linear motor for compressors of household refrigerators'. Proc. LDIA'2001, Nagano, Japan, 2001, pp. 283–286

[2] UTSUNO M., TAKAI M., YAEGASHI T., *ET AL.*: 'Efficiency characteristics of a linear oscillatory actuator under simulated compressor load'. Proc. LDIA'2001, Nagano, Japan, 2001, pp. 264–267

[3] HOWE D., ZHU Z.Q., CLARK R.E.: 'Status of linear drives in Europe'. Proc. LDIA'2001, Nagano, Japan, 2001, pp. 468–473

[4] VAN ZYL A.W., JEANS C.G., CRUISE R.J., LANDY C.F.: 'Comparison of force to weight ratios between a single-sided linear synchronous motor and a tubular linear synchronous motor'. Proc. IEEE Int. Electric Machines and Drives Conf. (IEMDC'1999), Seattle, USA, 1999, pp. 571–573

[5] BIANCHI N., BOLOGNANI S., CORTE D., TONEL F.: 'Tubular linear permanent magnet motors: an overall comparison', *IEEE Trans. Ind. Appl.*, 2003, **39**, (2), pp. 466–475

[6] EASTHAM J.F.: 'Novel synchronous machines: linear and disc', *IEE Proc. B*, 1990, **137**, (1), pp. 49–58

[7] WANG J., JEWELL G.W., HOWE D.: 'A general framework for the analysis and design of tubular linear permanent magnet machines', *IEEE Trans. Magn.*, 1999, **35**, (3), pp. 1986–2000

[8] WANG J., JEWELL G.W., HOWE D.: 'Design optimization and comparison of tubular permanent magnet machine topologies', *IEE Proc., Electr. Power Appl.*, 2001, **148**, (5), pp. 456–464

[9] WANG J., HOWE D.: 'Analysis of axially magnetised, iron-cored, tubular permanent magnet machines', *IEE Proc., Electr. Power Appl.*, 2004, **151**, (2), pp. 144–150

[10] LEQUESNE B.: 'Fast-acting long-stroke bistable solenoids with moving permanent magnets', *IEEE Trans. Ind. Appl.*, 1990, **26**, (3), pp. 401–407

[11] LEQUESNE B.: 'Permanent magnet linear motors for short stroke', *IEEE Trans. Ind. Appl.*, 1996, **32**, (1), pp. 161–168

[12] WANG J., HOWE D.: 'Design optimization of radially magnetized, iron-cored, tubular permanent magnet machines and drive systems', *IEEE Trans. Magn.*, 2004, **40**, (5), pp. 3262–3277

[13] WANG J., WANG W., JEWELL G.W., HOWE D.: 'Design and experimental characterization of a linear reciprocating generator', *IEE Proc., Electr. Power Appl.*, 1998, **145**, (6), pp. 509–518

[14] WANG J., HOWE D.: 'Tubular modular permanent-magnet machines equipped with quasi-Halbach magnetized magnets – part I: magnetic field distribution, EMF and thrust force', *IEEE Trans. Magn.*, 2005, **41**, (9), pp. 2470–2478

[15] HOGANAS: 'Somaloy$^{TM}$ brochure', available at: www.hoganas.com

[16] WANG J., HOWE D., JEWELL G.W.: 'Fringing in tubular permanent magnet machines: Part I – magnetic field distribution, flux-linkage and thrust force', *IEEE Trans. Magn.*, 2003, **39**, (6), pp. 3507–3516

[17] CHAI J., WANG J., HOWE D.: 'Evaluation of eddy current loss in tubular permanent magnet motors by three-dimensional finite element analysis'. Proc. XVII Int. Conf. Electrical Machines (ICEM2006), Paper ID: PSA1-12, Chania, Greece, 2–5 September 2006



doi: 10.1049/iet-epa:20070281